PNAS RESEARCH ARTICLE | NEUROSCIENCE OPEN ACCESS

IGF-1 receptor regulates upward firing rate homeostasis via the mitochondrial calcium uniporter

Maxim Katsenelson[a,b], Ilana Shapira[a], Eman Abbas[c,d,e], Kristina Jevdokimenko[c,d,e], Boaz Styr[a,1], Antonella Ruggiero[a], Saba Aïd[f], Eugenio F. Fornasiero[c,d,e], Martin Holzenberger[f], Silvio O. Rizzoli[c,d,e], and Inna Slutsky[a,b,2]

Edited by Eve Marder, Brandeis University Department of Biology, Waltham, MA; received December 5, 2021; accepted June 15, 2022

Regulation of firing rate homeostasis constitutes a fundamental property of central neural circuits. While intracellular Ca^{2+} has long been hypothesized to be a feedback control signal, the molecular machinery enabling a network-wide homeostatic response remains largely unknown. We show that deletion of insulin-like growth factor-1 receptor (IGF-1R) limits firing rate homeostasis in response to inactivity, without altering the distribution of baseline firing rates. The deficient firing rate homeostatic response was due to disruption of both postsynaptic and intrinsic plasticity. At the cellular level, we detected a fraction of IGF-1Rs in mitochondria, colocalized with the mitochondrial calcium uniporter complex (MCUc). IGF-1R deletion suppressed transcription of the MCUc members and burst-evoked mitochondrial Ca^{2+} (mitoCa^{2+}) by weakening mitochondria-to-cytosol Ca^{2+} coupling. Overexpression of either mitochondria-targeted IGF-1R or MCUc in IGF-1R–deficient neurons was sufficient to rescue the deficits in burst-to-mitoCa^{2+} coupling and firing rate homeostasis. Our findings indicate that mitochondrial IGF-1R is a key regulator of the integrated homeostatic response by tuning the reliability of burst transfer by MCUc. Based on these results, we propose that MCUc acts as a homeostatic Ca^{2+} sensor. Faulty activation of MCUc may drive dysregulation of firing rate homeostasis in aging and in brain disorders associated with aberrant IGF-1R/MCUc signaling.

firing rate homeostasis | homeostatic plasticity | mitochonria | IGF-1 receptor | MCU

Significance

An emerging hypothesis is that neuronal circuits homeostatically maintain a stable spike rate despite continuous environmental changes. This firing rate homeostasis is believed to confer resilience to neurodegeneration and cognitive decline. We show that insulin-like growth factor-1 receptor (IGF-1R) is necessary for homeostatic response of mean firing rate to inactivity, termed "upward firing rate homeostasis." We show that its mechanism of action is to couple spike bursts with downstream mitochondrial Ca^{2+} influx via the mitochondrial calcium uniporter complex (MCUc). We propose that MCUc is a homeostatic Ca^{2+} sensor that triggers the integrated homeostatic response. Firing rate homeostasis may be the principal mechanism by which IGF-1R regulates aging and neurodevelopmental and neurodegenerative disorders.

Neural circuits are composed of a large number of dynamic elements at various levels of organization. The operation of a neuronal circuit depends on the interaction between the intrinsic properties of the individual neurons and the synaptic interactions that connect them into functional ensembles. While some aspects of synaptic and spiking activity are dynamic, others show remarkable stability over long time periods (1). Despite a large variability in synaptic and intrinsic parameters, firing rate distributions and their mean firing rate (MFR) are maintained at a specific set-point value during ongoing spontaneous activity. MFRs are typically restored even in the presence of large perturbations to activity rates and patterns. The renormalization of MFRs to a set-point value has been observed in response to activity-dependent perturbations in cortical and hippocampal networks grown ex vivo (2–6) and to sensory deprivation in V1 cortex in vivo (7–10). MFR homeostasis can be achieved by a wide repertoire of homeostatic processes, including adjustments of synaptic strength, intrinsic excitability, and excitation-to-inhibition balance (11–13). Dysregulation of homeostatic plasticity has been proposed to drive synaptic and cognitive deficits in distinct brain disorders, including neurodevelopmental disorders (14, 15) and neurodegenerative disorders like Alzheimer's disease (16, 17).

Despite significant progress in our understanding of neuronal homeostasis, how firing rates are sensed and how this information is converted into feedback signaling remain largely unknown. Intracellular somatic cytosolic [Ca^{2+}] (cytoCa^{2+}) has been proposed to serve as a proxy of spiking activity because of their tight coupling and is therefore modeled as a feedback control signal (18, 19). According to these models, deviations from a specific target cytoCa^{2+} induce changes in effector proteins that result in renormalization of firing properties to a set point value. Indeed, cytoCa^{2+} in excitatory neurons returns to set-point value following sensory deprivation in vivo (9, 20) and following neuronal inactivity ex vivo (4). However, the molecular mechanisms that maintain cytoCa^{2+} around a target value and mediate the coordinated homeostatic response to stabilize firing rate distributions are unknown.

Insulin-like growth factor-1 receptor (IGF-1R) signaling is a well-known, evolutionary-conserved pathway regulating brain development (21, 22) and aging (23–26). In the central nervous system, IGF-1/IGF-1R signaling is critical for experience-dependent synaptic and neuronal plasticity in sensory cortices (27–29), adult neurogenesis (30–32), synaptic

Author contributions: M.K., E.F.F., S.O.R., and I.Slutsky designed research; M.K., I.Shapira, E.A., K.J., and A.R. performed research; B.S., S.A., E.F.F., and M.H. contributed new reagents/analytic tools; M.K., I.Slutsky, E.A., K.J., and A.R. analyzed data; and M.K., S.O.R., and I.Slutsky wrote the paper.

The authors declare no competing interest.

This article is a PNAS Direct Submission.

[1]Present address: Helen Wills Neuroscience Institute and Department of Bioengineering, University of California, Berkeley, CA 94720.

[2]To whom correspondence may be addressed. Email: islutsky@tauex.tau.ac.il.

This article contains supporting information online at http://www.pnas.org/lookup/suppl/doi:10.1073/pnas.2121040119/-/DCSupplemental.

Published August 9, 2022.

vesicle release (33–35) and neuronal excitability (35, 36). Moreover, IGF-1R is an important modulator of mitochondrial Ca^{2+} ($mitoCa^{2+}$) levels in hippocampal neurons (34). As mitochondria are involved in neuronal Ca^{2+} homeostasis (37), we have hypothesized that IGF-1R is necessary for the integrated homeostatic response to activity perturbations.

To test this hypothesis, we examined here how IGF-1R affects spike-to-Ca^{2+} transfer functions that quantitatively describe the coupling between spikes and the compartment-specific Ca^{2+} events they evoke. The coupling was measured at two different Ca^{2+} compartments—cytosol and mitochondria—in soma of excitatory hippocampal neurons. Specifically, we aimed to examine the role of spike-to-$cytoCa^{2+}$ and spike-to-$mitoCa^{2+}$ in the MFR homeostatic response to inactivity at the network level. Our results demonstrate that somatic mitochondria selectively uptake Ca^{2+} evoked by spike bursts, but not by single spikes. Utilizing superresolution imaging and biochemistry, we detected a population of IGF-1–bound IGF-1Rs in neuronal mitochondria, colocalized with mitochondrial calcium uniporter (MCU) and other members of the MCU complex (MCUc). Deletion of IGF-1Rs did not alter spike-to-$cytoCa^{2+}$ coupling, but weakened burst-to-$mitoCa^{2+}$ coupling by downregulating transcription of several MCUc members. Moreover, while a pronounced increase in the fraction of spike bursts was detected in the initial phase of the perturbation, this change in spike pattern was lost in IGF-1R–deficient neurons. Reduction in burst fraction and in burst-to-$mitoCa^{2+}$ coupling resulted in impaired MFR compensation in response to inactivity. Overexpression of either MCUc or mitochondria-targeted IGF-1R (mitoIGF-1R) in IGF-1R–KO neurons was sufficient to rescue both $mitoCa^{2+}$ and MFR homeostatic response. These results provide direct evidence for the critical role of IGF-1R/MCUc signaling in upward MFR homeostasis at the population level in hippocampal networks.

Results

IGF-1R Deficiency Limits Homeostatic Compensation of Mean Firing Rate and Pattern to Inactivity. To explore the role of $mitoCa^{2+}$ in MFR homeostasis, we first tested whether IGF-1R is necessary for the homeostatic regulation of firing rate distributions and their means. For this, we used multielectrode arrays (MEAs) for long-term recordings of spiking activity at the same cultured hippocampal neurons during baseline and throughout two days of activity perturbation. The $GABA_B$ receptor agonist baclofen (Bac) was used as a persistent inhibitory perturbation (4). For conditional deletion of IGF-1Rs, we used $IGF\text{-}1R^{fl/fl}$ mice (38) with a viral delivery of Cre-recombinase. We used adeno-associated virus (AAV) under the general promoter CBAP (AAV1/2-CBAP-Cre-Cerulean), creating IGF-1R knockout (IGF-1R–KO) networks (*SI Appendix*, Fig. S1 *A* and *B*). For control (Ctrl) experiments, $IGF\text{-}1R^{fl/fl}$ cultures were infected with AAV1/2-CBAP-Cerulean. As expected from our early work (4, 6), Ctrl networks displayed a pronounced suppression of activity by baclofen (10 μM) that was restored to the network's baseline MFR after a period of two days (Fig. 1 *A*–*C*). Conversely, the average firing rates of IGF-1R–KO networks exhibited only partial (~45%) recovery subsequent to baclofen application (Fig. 1 *D*–*F*). Moreover, distributions of Ctrl single-unit firing rates were indistinguishable before, and two days after, baclofen application (Fig. 2*A*). While effects of 2 d baclofen were variable per single unit in Ctrl conditions (Fig. 2*B*), on average per-unit MFR was not different following baclofen application (Fig. 2*C*). In contrast, MFR distribution was left-shifted following baclofen application in IGF-1R–KO neurons (Fig. 2*D*)

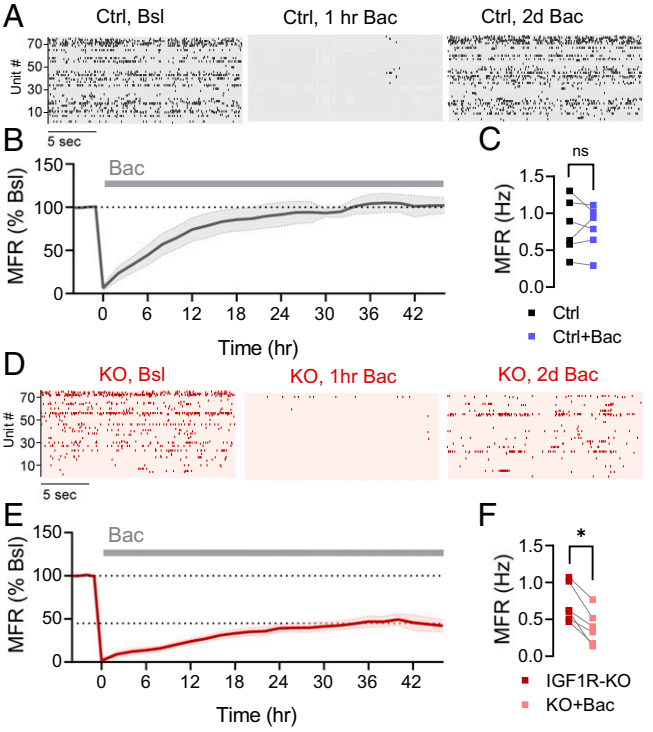

Fig. 1. IGF-1R deletion limits mean firing rate homeostasis at the network level. (*A*) Raster plots of the same neurons during baseline (Bsl, *Left*), acute application of 10 μM baclofen (Bac, *Center*), and following two days of Bac (*Right*) in Ctrl (Ctrl) cultures. (*B*) A typical MFR homeostatic response to chronic inactivity induced by 10 μM baclofen in Ctrl cultures, showing renormalization to the baseline network MFR (6 experiments, 535 units). (*C*) Summary of full MFR recovery following two days of Bac (Bac_{2d}) in Ctrl networks ($P = 0.68$, each point represents individual experiment, same data as *B*). (*D*) Raster plots of the same neurons during baseline (*Left*), acute application of Bac (*Center*), and following Bac_{2d} (*Right*) in IGF-1R–KO culture. (*E*) MFR homeostatic response was limited by IGF-1R–KO (6 experiments, 371 units). (*F*) Summary of partial recovery of MFRs following Bac_{2d} in IGF-1R–KO networks ($P = 0.0313$, each point represents individual experiment, same data as *E*). Wilcoxon test (*C* and *F*). Error bars indicate SEM. ns, not significant, $*P < 0.05$.

due to incomplete single-unit recovery (Fig. 2 *E* and *F*). In addition to changes in mean rate, temporal spike pattern was also affected by baclofen, confirming our early study (4). Namely, in Ctrl networks, the fraction of spikes participating in single-unit bursts (Fig. 2 *G* and *H*) and burst frequency normalized to MFR (*SI Appendix*, Fig. S2 *A* and *B*) showed an acute decrease and subsequent increase beyond the baseline level, which gradually declined during the perturbation. In contrast, IGF-1R–KOs showed lower fraction of spikes participating in bursts at any given moment of time: baclofen caused an acute decrease in the fraction of spikes in bursts that recovered to the baseline during the first day of the perturbation and eventually declined below the baseline during the second day of the perturbation (Fig. 2 *G* and *H*). These experiments point toward IGF-1R as a necessary component of homeostatic regulation of firing rate and pattern. Notably, IGF-1R deletion did not affect baseline firing rates (Fig. 2*I*) and patterns (Fig. 2 *J* and *K* and *SI Appendix*, Fig. S2 *E* and *F*), suggesting that IGF-1R is not necessary for the maintenance of baseline spontaneous network activity, but for the homeostatic response to chronic inactivity.

We next asked whether somatic $cytoCa^{2+}$ is also homeostatically regulated, and whether IGF-1R is necessary for this process. Continuous imaging of somatic $cytoCa^{2+}$ during spontaneous spiking activity in excitatory hippocampal neurons was conducted at baseline and following 2 d of baclofen perturbation

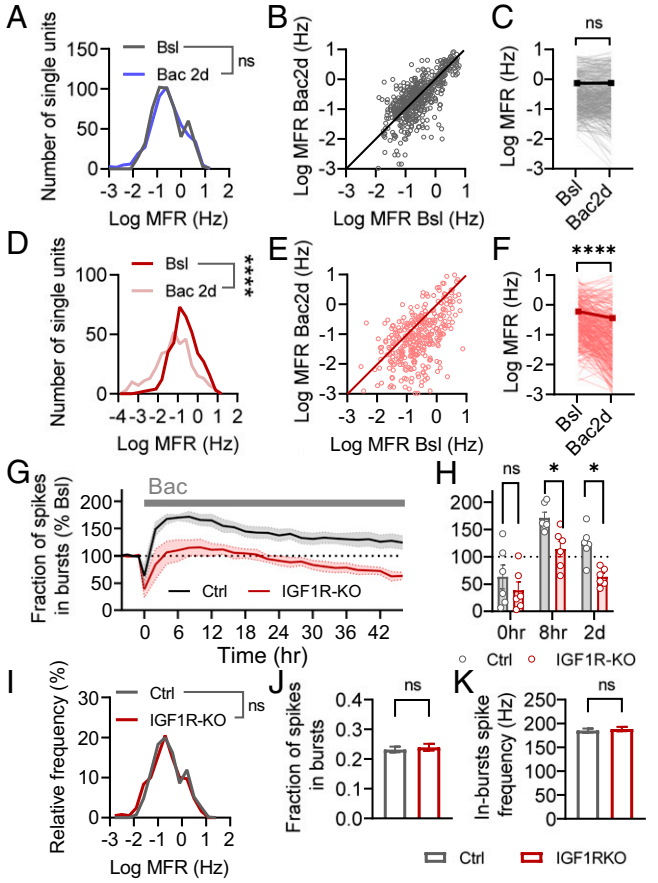

Fig. 2. Deletion of IGF-1R limits firing rate and pattern homeostasis, without affecting their basal metrics. (*A–C*) Effect of Bac_{2d} on 535 single units in Ctrl cultures. (*A*) Firing rate distributions were unchanged following Bac_{2d} ($P = 0.23$). (*B*) Changes in MFR per neuron. Line indicates no change. (*C*) MFRs were unchanged following Bac_{2d} ($P = 0.79$). (*D–F*) Effect of Bac_{2d} on 371 single units in IGF-1R–KO cultures. (*D*) Firing rate distributions were left-shifted following Bac_{2d}. (*E*) Changes in MFR per neuron. Line indicates no change. (*F*) MFRs were reduced following Bac_{2d}. (0.60 ± 0.05 Hz for IGF-1R–KO, 0.35 ± 0.05 Hz for KO+Bac). (*G* and *H*) Fraction of spikes participating in bursts following Bac_{2d} in Ctrl and IGF-1R–KOs ($n = 6$ experiments, 535 units in Ctrl; $n = 6$ experiments, 371 units in IGF-1R–KO). (*I–K*) IGF-1R–KO does not affect basal firing properties (same data as in *A–F*). No difference was found in MFR distributions between Ctrl and IGF-1R–KO neurons (*I*, $P = 0.1$), in fraction of spikes participating in bursts (*J*, $P = 0.31$, 0.23 ± 0.01 for Ctrl, 0.24 ± 0.01 for IGF-1R–KO) and in the intraburst spike frequency (*K*, $P = 0.32$, 185.1 ± 4.1 Hz for Ctrl, 188.4 ± 4.7 Hz, for IGF-1R–KO). Wilcoxon test (*C* and *F*), Kolmogorov-Smirnov test (*A*, *D* and *I*), Mann–Whitney *U* test (*J* and *K*), Two-way ANOVA with Sidak's multiple comparison test (*H*). Error bars indicate SEM. ns, not significant, *$P < 0.05$, ****$P < 0.0001$.

(*SI Appendix*, Fig. S1 *C* and *D*). The average amplitude, frequency, and Ca^{2+} influx index (a product of average amplitude x frequency) of cytosolic events were quantified for Ctrl and IGF-1R–KO neurons. In Ctrl, 2 d of baclofen did not affect cytoCa^{2+} event amplitudes, rate, and subsequently the Ca^{2+} influx index (*SI Appendix*, Fig. S1 *E–G*). In IGF-1R–KO neurons, the amplitude of cytoCa^{2+} events remained unaltered following the perturbation, but their frequency was diminished, resulting in lower Ca^{2+} influx index following 2 d of the perturbation (*SI Appendix*, Fig. S1 *H–J*). These results are in line with the electrophysiological data showing limited recovery of both MFR and burst rate (Fig. 1 *E* and *F* and *SI Appendix*, Fig. S2 *A* and *B*). Moreover, these data further support somatic cytoCa^{2+} as a regulated variable maintained by a homeostatic system and demonstrate that IGF-1R deletion impairs this regulation.

IGF-1 is the principal ligand of the IGF-1R (39). To test if it is the necessary signal for IGF-1R to enable MFR homeostasis, we knocked-down IGF-1 using an AAV carrying a small-hairpin RNA against it (shIGF-1). shIGF-1 mimicked the effect of IGF-1R–KO, showing a limited compensatory MFR response to baclofen in comparison to a control vector carrying a scrambled sequence (shScr, *SI Appendix*, Fig. S3 *A* and *B*). These results indicate that MFR homeostatic response is mediated by IGF-1–activated IGF-1Rs.

To test if IGF-1R is necessary for MFR renormalization to a set-point value for bidirectional changes in activity, we induced chronic hyperactivity in IGF-1R–KO neurons by enhancing glutamate spillover by inhibiting glutamate transporters (40). Application of 10 μM TBOA, a competitive glutamate transporter antagonist (41), induced a transient increase in MFR that was gradually renormalized during the following 2 d to the set-point value (*SI Appendix*, Fig. S3 *C* and *D*). Taken together, these results indicate that IGF-1R is essential for upward but not for downward homeostatic restoration of MFRs.

IGF-1R Deletion Blocks Postsynaptic and Intrinsic Homeostatic Plasticity. MFR homeostasis is achieved by intrinsic and synaptic adaptations that act in a negative-feedback manner to counteract disturbances to ongoing activity (12). Is IGF-1R necessary for a single but crucial compensatory mechanism, or rather is it an up-stream regulator of distinct compensatory mechanisms? To address this question, we measured several parameters of intrinsic excitability and synaptic strength in excitatory neurons using whole-cell patch clamp. We first tested whether intrinsic excitability is changed after 2 d of baclofen. We elicited action potentials by injecting somatic currents ranging from zero to 600 pA (F-I curves) in the presence of postsynaptic receptor blockers in Ctrl (Fig. 3 *A* and *B*) and IGF-1R–KO (Fig. 3 *C* and *D*) excitatory neurons. In Ctrl, 2 d of baclofen elicited an increase in firing rate in response to current injections (Fig. 3 *A* and *B*) and augmented the maximal firing frequency (*SI Appendix*, Fig. S4*A*). However, this plasticity of intrinsic excitability was lost in IGF-1R–KO neurons, as reflected by the lack of change in the F-I curve (Fig. 3 *C* and *D*) and the maximal firing frequency (*SI Appendix*, Fig. S4*A*) in response to 2 d of baclofen. Input resistance, spike threshold voltage, spike amplitude and half-width were unaltered by 2 d of baclofen in either Ctrl or IGF-1R–KO groups (*SI Appendix*, Fig. S4 *B–E*), but the KO group exhibited increased input resistance (*SI Appendix*, Fig. S4*B*) and decreased action potential amplitude (*SI Appendix*, Fig. S4*D*). These changes, however, did not result in changes of spontaneous firing (Fig. 2*I*).

Next, we tested whether IGF-1R deletion alters presynaptic and postsynaptic adaptations to inactivity. Indeed, in Ctrl neurons, 2 d of baclofen elicited a marked increase in the amplitude of miniature excitatory postsynaptic currents (mEPSCs) (Fig. 3 *E* and *F*), whereas in IGF-1R–KO neurons this homeostatic postsynaptic plasticity was lost, reflected by the lack of baclofen effect on the mEPSC amplitude (Fig. 3 *E* and *G*). On the other hand, the mEPSC frequency was increased in both groups (*SI Appendix*, Fig. S4 *F* and *G*). To test if IGF-1R preserves the integrity of presynaptic compensatory mechanisms, we quantified presynaptic vesicle recycling directly using FM-based method (42). As baclofen-induced increase in mEPSC frequency is associated with an increase in synaptic release probability (4), we used FM1-43 to test if homeostatic increase in synaptic release probability remains intact in IGF-1R–KOs. In response to 2 d of baclofen perturbation, both Ctrl and IGF-1R–KOs exhibited increased presynaptic strength evoked by low-frequency stimulation (*SI Appendix*, Fig. S4 *H–J*) and decreased short-term synaptic facilitation evoked by

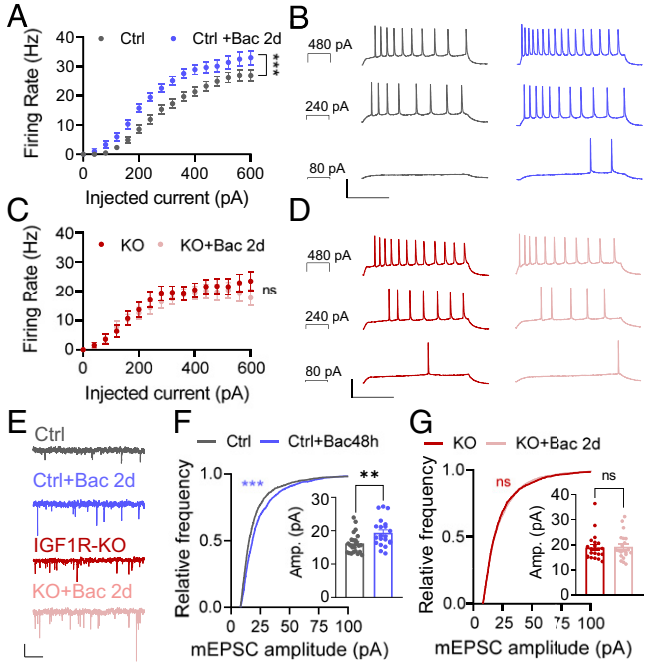

Fig. 3. Lack of intrinsic excitability and postsynaptic homeostatic adaptations in IGF-1R–KO neurons. (*A*) Increased firing of Ctrl neurons in response to depolarizing currents following Bac_{2d} (n = 29 for Ctrl, n = 24 for Ctrl+Bac). (*B*) Representative traces of Ctrl neurons before (Black) and after (Blue) Bac_{2d}. (*C*) No change (P = 0.56) in firing of IGF-1R–KO neurons in response to depolarizing currents following Bac_{2d} (n = 26 for IGF-1R–KO, n = 26 for KO+Bac). (*D*) Representative traces of IGF-1R–KO neurons before (Dark red) and after (Pink) Bac_{2d}. (*E*) Representative mEPSC recordings of neurons from each group (scale bars: 1 s, 20 pA). (*F*) Cumulative distribution of mEPSC amplitudes in Ctrl was skewed toward larger amplitudes following Bac_{2d} (n = 2,061 events from 23 Ctrl neurons and n = 1,887 events from 21 Ctrl+Bac neurons). *Inset*: mean of amplitudes is increased following Bac_{2d} (16.20 ± 0.64 pA, n = 23 for Ctrl; 19.37 ± 0.89 pA, n = 21 for KO+Bac). (*G*) Cumulative distribution of mEPSC amplitudes in IGF-1R–KO did not change following Bac_{2d} (P = 0.87, n = 1,860 events from 21 IGF-1R–KO neurons, 1,890 events from 21 KO+Bac neurons). *Inset*: mean of mEPSC amplitudes did not change (P = 0.87) following Bac_{2d} (18.92 ± 1.15 pA, n = 21 for IGF-1R–KO; 19.17± 1.12 pA, n = 21 for KO+Bac. Two-way ANOVA mixed-effects analysis (*A* and *C*), Kolmogorov-Smirnov and Mann–Whitney *U* tests (*F* and *G*). Error bars indicate SEM. ns, not significant, $^{**}P < 0.01$, $^{***}P < 0.001$.

high-frequency spike bursts (*SI Appendix*, Fig. S4 *K* and *L*), indicating an increase in release probability. These results suggest that IGF-1R is dispensable for the presynaptic homeostatic plasticity. However, the presynaptic compensation is insufficient for MFR renormalization. Taken together, our results demonstrate that deletion of IGF-1Rs impaired both postsynaptic and intrinsic homeostatic mechanisms that may contribute to the failure of MFR homeostatic recovery at the network level.

IGF-1R Deletion Suppresses Spike-to-MitoCa^{2+} Coupling. How changes in firing rates and patterns are translated into physiological error signals within neurons remains unknown. Somatic cytoCa^{2+} has long been assumed to be a regulated variable through which neurons sense changes in spiking activity, and by doing so are able to correct deviations from MFR set points (18, 19). Mitochondria are known to uptake Ca^{2+} upon neuronal activation (43), and thus may serve as a sensor of activity-induced changes in cytoCa^{2+} (17). As our early work found that IGF-1Rs modulate mitoCa^{2+} at the presynaptic compartment (34), we asked how do IGF-1Rs regulate activity-dependent cytoCa^{2+} and mitoCa^{2+} in neuronal soma. To address this question, we measured spike-to-cytoCa^{2+} and cyto-to-mitoCa^{2+} coupling for different patterns of spikes in Ctrl versus IGF-1R–KO excitatory neurons. We conducted simultaneous dual-color imaging of cytosolic and mitochondrial Ca^{2+} dynamics by using jRGECO1a and 4mt-GCaMP8m, respectively (Fig. 4*A*). To identify excitatory neurons, we used 4mt-GCaMP8m under the CaMKIIα promoter. Neurons were stimulated by a single spike and spike bursts comprising of 3, 5 and 10 spikes at 50 Hz, while spontaneous firing was blocked. Under these conditions, spike-to-cytoCa^{2+} coupling did not differ between Ctrl and IGF-1R–KO neurons (Fig. 4 *B* and *D*). Conversely, IGF-1R deletion caused a significant reduction in spike-to-mitoCa^{2+} coupling (Fig. 4 *C* and *E*). Importantly, mitoCa^{2+} transients were activated only by spike bursts, but not by single spikes. Hence, IGF-1R deletion diminished Ca^{2+} uptake by mitochondria evoked by spike bursts only. These changes resulted in weaker cytoCa^{2+}-to-mitoCa^{2+} coupling, as seen by the right-shift of their transfer function (Fig. 4*F*).

Given the central role of mitochondria in ATP production, we tested whether IGF-1R deletion suppressed ATP homeostasis. We used the cytosolic FRET sensor ATeam (44) to estimate somatic ATP levels in Ctrl and IGF-1R–KO hippocampal neurons. Our results show no difference in FRET efficiency by IGF-1R deletion during spontaneous activity (*SI Appendix*, Fig. S5). Taken together, these data suggest that IGF-1R–KO impairs somatic Ca^{2+} uptake by mitochondria, without affecting cytoCa^{2+} and ATP levels. The decreased mitoCa^{2+} transients elicited by burst-induced cytoCa^{2+} events, ultimately lead to a weakening of cytoCa^{2+}-to-mitoCa^{2+} coupling.

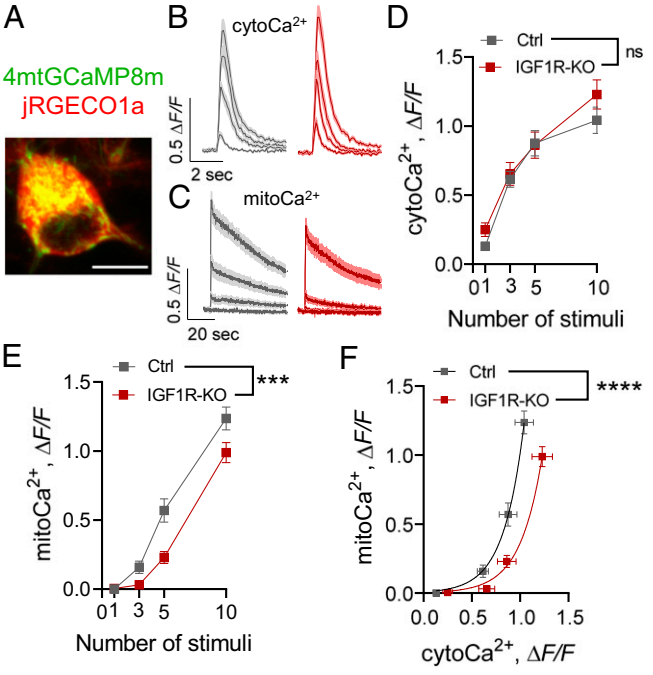

Fig. 4. IGF-1R deletion decreases somatic mitoCa^{2+} and cytoCa^{2+}-to-mitoCa^{2+} coupling evoked by spike bursts. (*A*) An excitatory neuron expressing cytosolic jRGECO1a and mitochondrial GCaMP8m. Scale bar: 10 μm. (*B*) Mean (dark line) and SEM of cytoCa^{2+} traces for a single spike and spike bursts composed of 3, 5, and 10 stimuli at 50 Hz. Scale bars: 0.5 ΔF/F, 2 s (*C*) Mean (dark line) and SEM of mitoCa^{2+} traces for a single spike and spike bursts composed of 3, 5, and 10 stimuli at 50 Hz. Scale bars: 0.5 ΔF/F, 20 s (*D*) cytoCa^{2+} responses were not changed (P = 0.42) by deletion of IGF-1R (n = 40–42 for Ctrl, n = 32–37 for IGF-1R–KO). (*E*) mitoCa^{2+} transients evoked by spike bursts were reduced in IGF-1R–KO neurons (n = 40–42 for Ctrl, n = 32–37 for IGF-1R–KO). (*F*) cytoCa^{2+}-to-mitoCa^{2+} coupling was reduced in IGF-1R–KO (n = 165 events for Ctrl, n = 142 events for IGF-1R–KO). Squares are mean of cytoCa^{2+} events from *D* and mean of mitoCa^{2+} events from *E*. Two-way ANOVA mixed effects analysis (*D* and *E*), Least square exponential regression. Extra sum-of-squares F test (*F*). Error bars indicate SEM. ns, not significant, $^{***}P < 0.001$, $^{****}P < 0.0001$.

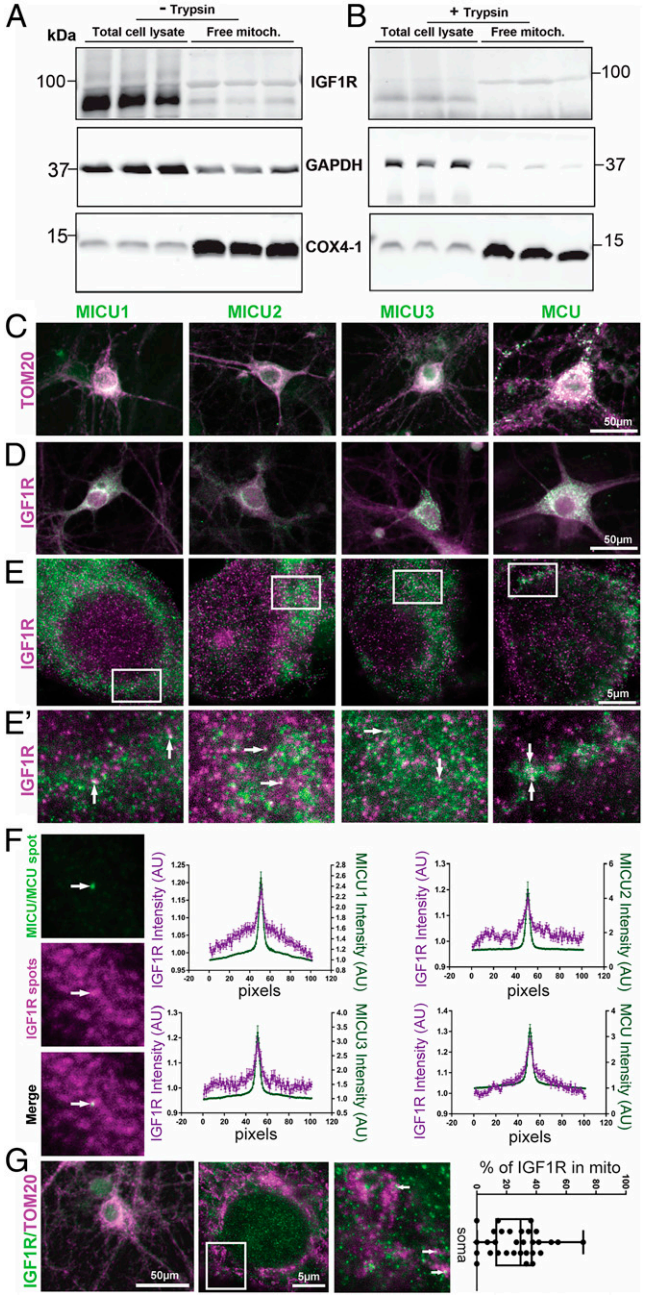

Fig. 5. IGF-1R is present in brain mitochondria, and is colocalized with MCUc within neurons. (*A*) Western blot (WB) analysis of mouse brain lysates and purified mitochondria (free mitochondria). The mitochondria are strongly enriched in the marker protein Cox4-1. The bands demonstrate the presence of the IGF-1R protein in or on mitochondria. (*B*) Samples were treated with trypsin to cleave all proteins from the outer membranes of the organelles in the samples. Remarkably, a prominent IGF-1R band is still visible in mitochondria after this treatment, suggesting that a significant proportion of IGF-1R is present within mitochondria. The experiments are shown in triplicate, to indicate experimental reproducibility. (*C*) Hippocampal cultured neurons were immunostained for TOM20, as a mitochondrial marker (magenta), in combination with antibodies against four different subunits of the MCUc (green). From left to right: MICU1, MICU2, MICU3, and MCU. Scale bars: 50 μm. The images were taken with an epifluorescence microscope. (*D*) Cultured neurons were immunostained as above, to test the colocalization of IGF-1R (magenta) and the respective MCUC subunits (green). Scale bars: 50 μm. (*E*) Representative STED images of neural cell bodies immunostained for IGF-1R (magenta) and MCUc subunits (green). (*E'*) Enlarged views of the delineated areas alongside the filled arrows depict examples of colabeling of IGF-1R and the MCUc proteins. Scale bars: 5 μm. (*F*) Square regions of interest (ROIs) were obtained for all MCUc spots, both in the MCUc and in the IGF-1R channels. The ROIs were then overlaid, which provides a visual indication of the presence of IGF-1R in relation to MCUc spots. The arrows point to the ROI centers, where the MCUc spots are located, and where an enrichment of IGF-1R is also observed. To analyze these images, line scan profiles of intensity for IGF-1R (magenta) and the four MCUc subunits (green) were performed across the ROIs, and are shown as means ± SEM from 8 samples for each MCUc subunit. A small, but significant enrichment of IGF-1R near MCUc spots can be observed for all samples (Kruskal-Wallis tests followed by a post hoc Tukey test, corrected for multiple comparisons; $P < 0.001$ for colocalization with MCU, MICU1 and MICU2; $P < 0.05$ for MICU3). (*G*) We immunostained the cultured neurons for IGF-1R (green) and the mitochondrial marker TOM20 (magenta), to estimate the proportion of IGF-1R that colocalizes with mitochondria. STED images strongly suggest a partial colocalization in the soma (some colocalized molecules are shown by the arrows). Scale bars, 50 μm and 5 μm, respectively. The quantification shows the percentage of IGF-1R spots found within the space delimited by the TOM20 staining (i.e., found on mitochondria), which averages to ~30%. The box shows the median and the quartiles, while the whiskers show the range of data ($n = 5$ independent experiments, with 5–7 cells imaged for each experiment).

IGF-1R Is Present in Neuronal Mitochondria. The mechanism used by IGF-1R to regulate the mitoCa^{2+} influx does not appear to be straightforward, when one considers that IGF-1R is a canonical plasma membrane receptor. One solution to this problem would be the presence of IGF-1R in mitochondria, where the MCUc is located. We tested this by biochemical fractionation and superresolution imaging approaches (Fig. 5). Using an antibody against the β subunit of IGF-1R, we detected the unmodified IGF-1R β subunit (~95 kDa), which was predominant in the total lysate of mouse brain, and an additional ~100-kDa band that was enriched in the mitochondrial fraction (Fig. 5*A*). This second band was stable when the lysates were treated with trypsin, implying that a fraction of IGF-1R is found in the inner mitochondrial space, and is not simply attached to the outer mitochondrial membrane (Fig. 5*B*). Next, we tested whether IGF-1R is colocalized in mitochondria with MCUc, using 2-color stimulated emission depletion (STED) microscopy (Fig. 5 *C* and *D*). This revealed a partial colocalization of IGF-1R and the four MCUc components - the pore-forming subunit MCU, as well as regulatory subunits MICU1, MICU2 and MICU3 (Fig. 5 *E* and *E'*). Quantitative analysis indicated that the colocalization is statistically significant, with the IGF-1R signal in the MCUc spots being significantly higher than elsewhere (Fig. 5*F*). On average, ~30% of IGF-1Rs in soma are localized with the bona fide mitochondrial marker TOM20 (Fig. 5*G*). Finally, we tested if mitochondrial IGF-1R binds IGF-1 using a proximity ligation assay (PLA, see *SI Appendix, Methods*). The PLA allows visualization of the interaction between two endogenous proteins in fixed neurons strictly dependent on the simultaneous recognition of the target by two antibodies (*SI Appendix, Methods*). As shown in *SI Appendix*, Fig. S6, ~40% of IGF-1Rs bound to IGF-1 were localized to the mitochondria. Taken together, these results suggest that IGF-1–bound IGF-1Rs are present in the mitochondria, where it colocalizes with MCUc complexes.

Rescue of MitoCa^{2+} and Upward MFR Homeostatic Response by MitoIGF-1R/MCUc. Given that MCUc is the primary Ca^{2+} source into mitochondria (37), reduction in mitoCa^{2+} by IGF-1R deletion may result from down-regulation of the MCUc subunits. To test this hypothesis, we measured the mRNA expression levels of MCU and the Ca^{2+}-sensing subunits MICU1, MICU2 and MICU3. We found that IGF-1R deletion caused a down-regulation in the expression level of MCU and the brain-specific (45) MICU3 subunits, while it did not affect the expression levels of MICU1 and MICU2 subunits (Fig. 6*A*). We therefore conclude that IGF-1R affects MCU and MICU3 expression at the transcriptional level.

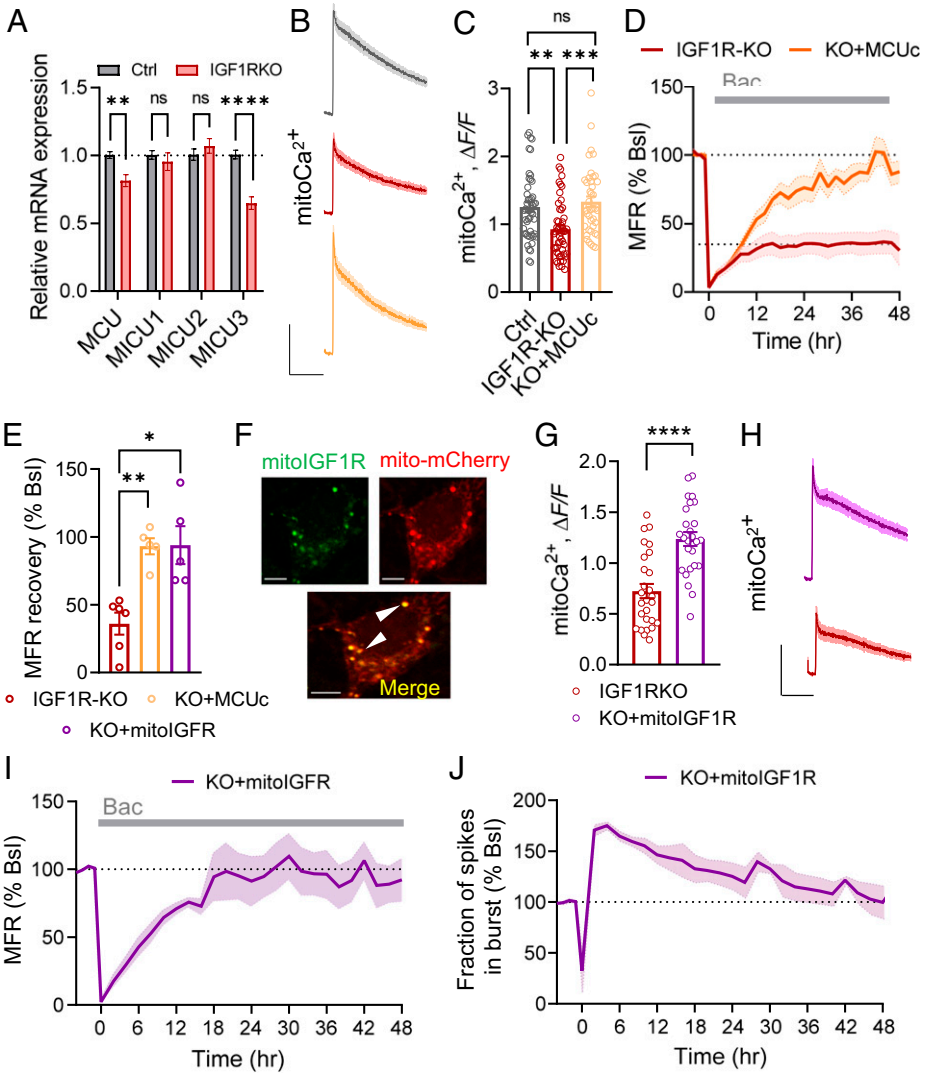

Fig. 6. Over-expression of mitoIGF-1R or MCUc rescues mitoCa^{2+} and MFR homeostasis in the absence of IGF-1R. (*A*) mRNA expression of MCUc proteins in IGF-1R–KO cultures relative to Ctrl: The mRNA of MCU and MICU3 was reduced in IGF-1R–KO culture (0.815 ± 0.045 for MCU; 0.649 ± 0.046 for MICU3), and did not change in MICU1 and MICU2 (0.954 ± 0.064, $P = 0.925$ for MICU1; 1.070 ± 0.054, $P = 0.832$ for MICU2, $n = 15$ for IGF-1R–KO; $n = 13$ for Ctrl. Samples from 3 experiments for MCU and MICU3, samples from 2 experiments ($n = 9$) for MICU1 and MICU2). (*B*) Mean (dark line) and SEM of mitoCa^{2+} event traces in response to 10 stimuli at 50 Hz shown in *C*. (*C*) MitoCa^{2+} is reduced by IGF-1R deletion, and is rescued by over-expression of MCUc in IGF-1R–KO neurons ($P > 0.99$, 1.25 ± 0.07, $n = 49$ for Ctrl; 0.93 ± 0.06, $n = 52$ for IGF-1R–KO, 1.33 ± 0.08, $n = 42$ for KO+MCUc). (*D*) Impaired MFR response to chronic inactivity induced by 10 μM baclofen in IG1R–KO cultures expressing mCherry, normalized to the baseline MFR (red line, 6 experiments, 291 channels). Restoration of a normal MFR homeostatic response in IGF-1R–KO+MCUc, normalized to the baseline MFR (orange line, 5 experiments, 252 channels). (*E*) Summary (same data as *D* and *I*) shows restoration of MFR recovery following Bac_{2d} by MCUc or mitoIGF-1R in IGF-1R–KO (93.1 ± 5.9% of baseline for IGF-1R–KO+MCUc and 93.9 ± 13.9% for IGF-1R–KO+mitoIGF-1R, compared to 36.1 ± 8.0% for IGF-1R–KO+mCherry). Each circle is the mean of the last four time-points of each experiment in *D* and *I*. (*F*) Representative confocal images of a hippocampal neuron expressing mitoIGF-1R (4mtIGF-1R–mTagBFP2, *Top Left*), mito-mCherry (2mt-mCherry, *Top Right*) and the merged image of both markers showing overlapping expression (*Bottom*). Arrows show examples of mitoIGF-1R and mito-mCherry colocalization. Scale bar: 5 μm. (*G*) Expression of mitoIGF-1R in IGF-1R–KO neurons increased mitoCa^{2+} in response to 10 stimuli at 50 Hz (0.72 ± 0.07, $n = 27$ for IGF-1R–KO, 1.24 ± 0.07, $n = 26$ for KO+mitoIGF-1R). (*H*) Mean (dark line) and SEM of mitoCa^{2+} event traces in (*F*) scale bars: 20 s, 0.5 Δ*F*/*F*. (*I*) Normal MFR homeostatic response in IGF-1R–KO+mitoIGF-1R, normalized to the baseline MFR (5 experiments, 458 channels). (*J*) Fraction of spikes participating in bursts following Bac_{2d} in IGF-1R–KOs expressing mitoIGF-1R ($n = 4$ experiments, 421 units). Two-way ANOVA with Sidak's multiple comparison test (*A*), Kruskal-Wallis test with Dunn's correction for multiple comparisons (*B* and *E*), Mann–Whitney *U* test (*H*). Error bars indicate SEM. ns, not significant, *$P < 0.05$, **$P < 0.01$, ***$P < 0.001$, ****$P < 0.0001$.

To directly test whether reduction in mitoCa^{2+} is the primary cause of impaired MFR homeostasis in IGF-1R–KOs, we tested whether ectopic overexpression of MCUc may rescue mitoCa^{2+} and MFR homeostasis. Our results show that overexpression of MCU, together with its regulatory subunits (MICU1 and MICU3), led to an increase in mitoCa^{2+} transients evoked by spike bursts in IGF-1R–KOs, rescuing it to control level (Fig. 6 *B* and *C*). Then, we tested if the rescue of mitoCa^{2+} in IGF-1R–KO neurons is sufficient to restore MFR homeostasis in response to inactivity. While MFR recovered only to 36% of the baseline in IGF-1R–KO networks overexpressing mCherry, overexpression of MCUc markedly increased the compensatory response of IGF-1R–KO networks to 93% of the baseline (Fig. 6 *D* and *E*). As MCUc rescues both mitoCa^{2+} and MFR homeostasis in response to inactivity, these results strongly suggest that IGF-1R deletion impairs MFR homeostatic recovery from inactivity by reducing mitoCa^{2+} uptake during spike bursts.

Finally, we examined if restoring IGF-1R exclusively in the mitochondria is sufficient for functional recovery of mitoCa^{2+} dynamics and MFR homeostasis. To localize IGF-1R to mitochondria, we fused IGF-1R sequence at the N terminus to a tandem of four repeats of the Cox-8 mitochondria-targeting peptide

(AAV-CBAP–4mtIGF-1R–mTagBFP2, called mitoIGF-1R). MitoIGF-1Rs were colocalized with mitochondrial marker mito-mCherry in neurons (Fig. 6*F*). Expression of mitoIGF-1R in IGF-1R–KO neurons increased mitoCa^{2+} to Ctrl levels (Fig. 6 *G* and *H*) and rescued MFR homeostasis (Fig. 6 *I* and *E*). Furthermore, mitoIGF-1R expression rescued baclofen-induced change in spike pattern in IGF-1R–KOs; the fraction of spikes participating in single-unit bursts was increased above the baseline during the initial phase of the perturbation and gradually decreased to the baseline (Fig. 6*J*), similarly to control conditions (Fig. 2*G*). Thus, a subpopulation of IGF-1R, mitoIGF-1R, is sufficient for the proper functioning of both processes—mitoCa^{2+} and MFR homeostasis.

Discussion

Long-term stability of ongoing spiking dynamics is crucial for neural circuits' functions (46–50). Although a large number of fine-tuned parameters regulating synaptic and intrinsic membrane properties can generate similar firing properties (51, 52), the cellular and molecular design underlying MFR homeostasis in central neural networks remains largely unknown. Here, we identify a novel role of IGF-1Rs, known regulators of brain development (21), proteostasis (53, 54) and lifespan (23, 24, 26), in homeostasis of neural network activity. Our results provide converging evidence on the necessity of evolutionary-conserved IGF-1R signaling in the stabilization of firing rate distributions at the population level in hippocampal networks. These results are important for several reasons. First, they demonstrate that IGF-1Rs are dispensable in regulating MFR set points during spontaneous neuronal activity, but are critical for the homeostatic compensation of MFR to inactivity. Second, they reveal a role of IGF-1R in regulating temporal Ca^{2+} filtering via MCUc of neuronal mitochondria during periods of spike bursts. Third, they reveal that a subpopulation of IGF-1Rs is present in mitochondria and colocalized with MCUc. Fourth, they show that either mitoIGF-1R or MCUc can restore upward MFR homeostasis in IGF-1R–deficient networks. Finally, they point to a critical role of mitochondria in regulating the integrated homeostatic response at the network level.

Mitochondria as High Pass Filters in Central Neurons. Our results indicate that neurons are extremely unreliable at transferring information encoded by single spikes to somatic mitochondria. The coupling of mitochondria-to-cytosolic Ca^{2+} is nonlinear, showing almost complete uncoupling during periods of low-frequency, single spikes. However, spike bursts, known to play an important role in synaptic plasticity and information processing (55), are reliably signaled to mitochondria by activating mitoCa^{2+} influx via MCUc. Thus, neuronal mitochondria can be viewed as filters that transmit bursts, but filter out single spikes. Our results demonstrate that these filter properties are regulated by IGF-1Rs. We identified a subpopulation of IGF-1Rs that localizes in mitochondria and regulates mitoCa^{2+} entry in hippocampal neurons. While previous work identified several other members of receptor tyrosine kinase family that can translocate to mitochondria, such as EGFR (56, 57) and ErbB2R (58), future studies are needed to understand the mechanism of IGF-1R translocation to neuronal mitochondria and its posttranslational modifications. Similarly to EGF (57), IGF-1 may induce internalization and translocation of the IGF-1R from the plasma membrane to the mitochondria (*SI Appendix*, Fig. S7). Irrespective of the precise mechanism, our results point to mitoIGF-1R as a key regulator of mitoCa^{2+} influx. Although our conclusions are based on cultured neurons, a recent in vivo study in the cortex of awake mice showed a positive relationship between mitoCa^{2+} and cytoCa^{2+} peak amplitudes, wherein large cytoCa^{2+} events are likely to be evoked by spike bursts (59). Therefore, unreliable spike-to-mitoCa^{2+} coupling during single spikes appears to be a universal property of somatic mitochondria in central neurons. Given that the duration of mitoCa^{2+} events is ∼8 times longer than cytoCa^{2+}, mitochondria perform amplification and high-pass filtering of burst-evoked cytoCa^{2+} signals. Therefore, MCUc does not only sense cytoCa^{2+} to control the threshold and gain as has been previously proposed (60), but also controls information content transferred from cytoplasmic membrane potential to mitochondria.

MCUc as a Homeostatic Sensor. What is the role of IGF-1R/MCUc signaling in upward MFR homeostasis? Here, we propose that MCUc is a homeostatic sensor that drives expression of intrinsic and postsynaptic homeostatic plasticity, and eventually MFR homeostatic response (*SI Appendix*, Fig. S7). MCUc senses the changes in cytoCa^{2+} by Ca^{2+}-binding EF-hand-containing regulatory subunits MICU (61). At the resting level of cytoCa^{2+}, MICU1-MICU2 and MICU1-MICU3 heterodimers prevent ion conduction through the MCU channel, and they permit it when Ca^{2+} levels rise (62). Our results indicate that the rise of cytoCa^{2+} evoked by spike bursts is sufficient to activate MCUc in neuronal soma. Our current and previous (4) results demonstrate that $GABA_BR$-mediated suppression of MFR is associated with a change in temporal spike pattern: the fraction of spike participating in bursts is increased during the initial phase of the perturbation. These changes in the temporal spike structure promote a more efficient activation of MCUc during the induction phase of homeostatic plasticity. The function of IGF-1Rs in upward MFR homeostasis is two-fold: 1) to enable an increase in the fraction of spike bursts during the induction phase of homeostatic plasticity; 2) to maintain burst-to-mitoCa^{2+} coupling. Either reduction in secretion of IGF-1 or in IGF-1R expression level may decrease MCUc activation and thus impair the induction of intrinsic and postsynaptic homeostatic plasticity. Importantly, expression of mitoIGF-1Rs in IGF-1R–KO neurons rescued all 3 components: baclofen-induced increase in the fraction of spike bursts, burst-to-mitoCa^{2+} coupling and upward MFR homeostasis. Thus, mitoIGF-1R signaling emerges as a critical element in the induction of the integrated MFR response by regulating spike pattern and burst-to-mitoCa^{2+} coupling (*SI Appendix*, Fig. S7). As IG1-R does not alter presynaptic homeostatic plasticity, other homeostatic sensors, such as the endoplasmic reticulum (ER) Ca^{2+} sensor MCTP may drive presynaptic homeostasis (63). It remains to be tested if IGF-1 serves as a permissive cue as suggested for other secreted factors (64–66) and if burst-to-mitoCa^{2+} uncoupling limits MFR compensation to other inactivity perturbations associated with suppression of spike burst fraction, such as AMPA receptor blockade (4).

Spike bursts are known to induce frequency- and spike-timing dependent plasticity (67). Moreover, recent findings demonstrate that spike bursts evoke pronounced mitoCa^{2+} transients in soma and apical dendrites (68) and mitoCa^{2+} is implicated in the induction of long-term potentiation (69). What are the mechanisms that separate the functions of burst-induced mitoCa^{2+} in Hebbian vs. homeostatic plasticity? One possibility is that different sources of Ca^{2+} entry to the cytosol are coupled to different intracellular signaling pathways. While Ca^{2+} entry trough NMDARs is critical for induction of Hebbian-like synaptic plasticity (70), Ca^{2+} entry through L-type (71, 72) and

T-type (73) voltage-gated calcium channels has been implicated in homeostatic plasticity. Moreover, the impact of N-type calcium channels on transcription is proposed to depend on Ca^{2+} buffering via mitochondria and ER (74). Thus, IGF-1R–depedent mitoCa^{2+} may regulate MFR homeostasis by tuning spike bursts - transcription coupling. How IGF-1R/MCUc signaling regulates mitochondria-to-nucleus Ca^{2+} coupling and transcriptional programs related to the upward MFR homeostatic response remains a challenge for future research.

IGF-1R and MFR Homeostasis. The network's ability to yield the same output despite different molecular compositions, called degeneracy, is proposed to be a ubiquitous biological property at all levels of organization (75). However, homeostatic regulation may fail when one of the core homeostatic machinery components becomes dysfunctional (16). Here, we show that IGF-1R deficiency limits upward firing rate homeostasis by suppressing mitoCa^{2+}-to-cytoCa^{2+} coupling via MCUc. Thus, in addition to cytoCa^{2+}, mitoCa^{2+}-to-cytoCa^{2+} coupling may play a crucial role in MFR homeostasis.

It has been recently demonstrated that the loss of Shank3, implicated in autism spectrum disorders, impairs upward MFR homeostasis and ocular dominance plasticity in the V1m cortex (76). Interestingly, injection of IGF-1 prevents effects of monocular deprivation on ocular dominance plasticity in the V1 cortex (28). Moreover, IGF-1 restored deficits in excitatory synaptic transmission in neurons with reduced Shank3 expression from 22q13 deletion syndrome patients (77). However, whether deficiency in mitoCa^{2+} evoked by spike bursts also limits upward MFR homeostasis in visual cortex and hippocampus in vivo is unknown. Whether common homeostatic mechanisms maintain stability of distinct neural circuits serving different functions remains an attractive question for future studies.

We hypothesize that maintaining a delicate balance of IGF-1R signaling is critical for normal brain functioning. On the one hand, some brain disorders are associated with down-regulation of IGF-1. For example, *Mecp2* mutant mice, a model of Rett syndrome, exhibit decreased levels of serum IGF-1 (78). A treatment of *Mecp2* mutant mice with systemic IGF-1 restored Rett syndrome-like symptoms, including synaptic and cognitive deficits (78, 79). As *Mecp2* deletion impairs homeostatic synaptic scaling (80, 81) and excitation-to-inhibition balance (82), it would be important to test if IGF-1 restores the symptoms by rescuing homeostatic failures. On the other hand, a decrease in IGF-1R signaling protects from amyloid-β-mediated pathology as well as from synaptic, neuronal and cognitive deficits in Alzheimer's disease mouse models (34, 53, 83, 84). Moreover, inhibition of MCU decreases mitoCa^{2+} overload in cortical neurons of Alzheimer's disease model mice (85). Reduced mitoIGF-1R/MCUc signaling may be neuroprotective by suppressing disease-associated hyperactivity of hippocampal synapses (34) and by restricting upward MFR homeostasis. It is noteworthy that the transcription factor REST regulates downward MFR homeostasis (86) and extends lifespan (87). It remains to be seen whether a critical role of IGF-1R in development and aging is rooted in its capacity to regulate firing rate homeostasis of central neural circuits.

Methods

Primary Hippocampal Culture Preparation. Hippocampal cultures were prepared from IGF-$1R^{fl/fl}$ (88) pups (both sexes) at P0-1 as described before (89). For all electrophysiology and live cell imaging, cultures were infected at 5–6 d in vitro (DIV) with Cre+ or Cre− AAVs, shScr or shIGF-1 AAVs, and with MCUc (MCU, MICU1 and MICU3) or mtIGF-1R on DIV 8&9 (MCU and MICU1 on day 8, and MICU3 on the next day). The experiments were performed in cultures after 14–21 DIV. See *SI Appendix, Methods* for plasmid construction.

Electrophysiology.

MEA data acquisition and analysis. Cells were grown on MEA plates [Multi Channel Systems (MCS), 120MEA200/30iR-Ti] containing 120 titanium nitride (TiN) electrodes with four internal reference electrodes. Data were recorded by either a MEA2100-System (MCS) with a chamber that maintained 37 °C and 5% CO_2, or a MEA1200-minisystem (MCS) that was constantly placed inside an incubator. Raw data were collected at 10 kHz, with a hardware high-pass filter of 1 Hz and an upper cutoff of 3.3 kHz for the MEA2100-system and 3.5 kHz for the MEA2100-minisystem. See *SI Appendix, Methods* for spike analysis.

Patch clamp whole-cell recordings and analysis. Experiments were performed at room temperature in a RC-26G recording chamber (Warner instrument LCC, USA) on the stage of FV300 inverted confocal microscope (Olympus, Japan) using a Multiclamp 700B amplifier and a Digidata 1440A digitizer (Molecular devices, LLC, USA). All experiments were carried out using extracellular Tyrode solution containing (in mM): NaCl, 145; KCl, 3; glucose, 15; Hepes, 10; $MgCl_2$, 1.2; $CaCl_2$, 1.2; pH adjusted to 7.4 with NaOH, and intracellular solution containing (in mM): K-gluconate 120; KCl 10; HEPESs 10; Na-phosphocreatine 10; ATP-Na_2 4; GTP-Na 0.3; $MgCl_2$ 0.5. Intracellular solution was supplemented with 20 μM Alexa fluor 488 for dendritic spines imaging. For intrinsic excitability, synaptic blockers were used (in μM): 10 CNQX, 50 AP-5, and 10 gabazine. For mEPSCs recordings, tetrodotoxin (1 μM), AP-5 (50 μM), and gabazine (10 μM) were added to Tyrode's solution. Signals were recorded at 10 kHz, and low-pass filtered with Bessel filter 2 kHz. Electrophysiological data were analyzed using pClamp (Molecular Devices LLC, USA) and MiniAnalysis (Synaptosoft, Decatur, Georgia, USA) for mEPSC. See all the details in the *SI Appendix, Methods*.

Confocal Live Cell Imaging.

Evoked cytosolic and mitochondrial calcium imaging in neuronal soma. Experiments were performed on a FV-1000 (Olympus, Japan) system using a QR/RC-47FSLP chamber with a TC-324C temperature controller (Warner Instruments LLC, USA) at 33–34 °C. In-chamber temperature stability was verified between coverslips with a Newtron TM-5005 thermometer. Coverslips were placed in Tyrode's solution that contained (in mM): NaCl, 145; KCl, 3; glucose, 15; Hepes, 10; $MgCl_2$, 1.2; $CaCl_2$, 1.2; pH adjusted to 7.4 with NaOH at 34 °C. Synaptic blockers were used to prevent recurrent activity from stimulation (in μM): 10 CNQX, 50 AP-5. Cultures were infected with AAV1/2-hSyn-jRGECO1a and AAV1/2-CaMKIIα-4mt-GCaMP8m, so that only excitatory neurons expressed both Ca^{+2} sensors. Only cells with mitochondrial response to a 10-stimuli burst at 50 Hz were considered. Infection with AAV1/2-CBAP-Cre-Cerulean or AAV1/2-CBAP-Cerulean was verified with a 440 nm laser. Imaging was done with a 60X lens and ×1.5 digital magnification at ∼12.5 frames per second with 488 nm and 561 nm lasers, and emission spectra of 505–540 nm and 575–675 nm for GCaMP8m and jRGECO1a, respectively. Field stimulation was given using a SIU-102 stimulation unit (Warner Instruments LLC, USA) connected to an Axon Digidata 1440A digitizer (Molecular devices, LLC, USA). Each imaged neuron was stimulated by a single stimulus and bursts of 3, 5 and 10 stimuli at 50 Hz. Some neurons had more than one clear response to 3, 5 or 10 stimuli and thus excluded from analysis. Analysis were done using ImageJ.

STED Microscopy. Immunostaining was carried out based on standard protocols (*SI Appendix*). The following primary antibodies were used: MICU1 rabbit polyclonal (1:100; Sigma), MICU2 rabbit polyclonal (1:50; Sigma), MICU3 rabbit polyclonal (1:150; Sigma), MCU rabbit polyclonal (1:100; Sigma), TOM20 mouse monoclonal (1:100; Sigma), and IGF-1Rβ mouse monoclonal (1:100; Invitrogen, 194Q13). The applied secondary antibodies were anti-mouse STAR580 and anti-rabbit STAR635P purchased from Abberior GmbH, Göttingen, Germany. Epifluorescence images (Fig. 5 *C* and *D*) were obtained by means of an IX83 inverted microscope (Olympus). STED imaging (Fig. 5 *E* and *E′*) was captured using a STED Abberior microscope, Göttingen, Germany. Excitation lines of 640 nm and 561 nm were adopted for exciting Star653P (MCUc subunits) and Star580 (TOM20 and IGF-1R). For STED excitation, pulsed lasers were set at 640 nm and 580 nm. STED depletion was implemented via 775 nm depletion laser and the images were acquired at 20 nm pixel size.

Brain and Free Mitochondria Purification. Brain lysates and free mitochondria were isolated as previously described (90) form 5-mo-old C57BL/6Rj with minor modifications (*SI Appendix*). These mitochondria were named "free mitochondria" and were used for further analyses.

Statistical Analysis. Experiments were repeated at least three times (three independent cultures) for each group. Data are shown as mean ± SEM (SEM). All statistical analyses were carried out using GraphPad Prism 8.0 (GraphPad software, USA), and the specific tests of each figure, along with their *P* values and total number of cells/repetitions per experimental group (n/N) are specified in the figure legends.

Data Availability. All study data are included in the article and/or supporting information.

ACKNOWLEDGMENTS. We thank Tim O'Leary and Lee Susman for comments on the manuscript, Leore R. Heim for graphical illustration, and all members of the I. Slutsky laboratory for discussions. We also thank Dr. Sven Dennerlein (University Medical Center Göttingen, Germany) for help with western blot experiments in mitochondria and for sharing precious reagents. This work was supported by research grants from the European Research Council (724866 to I. Slutsky), the Israel Science Foundation (1663/18 to I. Slutsky), the Volkswagen Foundation and the Ministry of Science and Culture of Lower Saxony (ZN3458 to I. Slutsky and S.O.R.), The Deutsche Forschungsgemeinschaft (440813539 to I. Slutsky and S.O.R., German indicator RI 1967/11-1, and 448865644 to I. Slutsky), BIRAX (the Britain Israel Research and Academic Exchange Partnership) Ageing Initiative (46BX18TKIS to I. Slutsky), the Israel Ministry of Science, Technology and Space (to I. Slutsky), and the Rosetrees Trust (A2590 to I. Slutsky). S.A. and M.H. received research funds from INSERM (National Institute of Health and Medical Research) and Sorbonne University. I. Slutsky is grateful to the Sheila and Denis Cohen Charitable Trust and the Rosetrees Trust of the United Kingdom for their support. M.K. is grateful to the Sagol School of Neuroscience for the award of a doctoral fellowship. This work was performed in partial fulfillment of the requirements for a PhD degree by M.K. at the Sackler Faculty of Medicine and the Sagol School of Neuroscience, Tel Aviv University, Israel.

Author affiliations: [a]Department of Physiology and Pharmacology, Sackler Faculty of Medicine, Tel Aviv University, 69978 Tel Aviv, Israel; [b]Sagol School of Neuroscience, Tel Aviv University, 69978 Tel Aviv, Israel; [c]Department of Neuro- and Sensory Physiology, University Medical Center Göttingen, 37073 Göttingen, Germany; [d]Center for Biostructural Imaging of Neurodegeneration (BIN), 37075 Göttingen, Germany; [e]Cluster of Excellence "Multiscale Bioimaging: from Molecular Machines to Networks of Excitable Cells" (MBExC), University of Göttingen, 37073 Göttingen, Germany; and [f]INSERM and Sorbonne University, Research Center UMR 938, 75012 Paris, France

1. A. R. Chambers, S. Rumpel, A stable brain from unstable components: Emerging concepts and implications for neural computation. *Neuroscience* **357**, 172–184 (2017).
2. G. G. Turrigiano, K. R. Leslie, N. S. Desai, L. C. Rutherford, S. B. Nelson, Activity-dependent scaling of quantal amplitude in neocortical neurons. *Nature* **391**, 892–896 (1998).
3. J. Burrone, M. O'Byrne, V. N. Murthy, Multiple forms of synaptic plasticity triggered by selective suppression of activity in individual neurons. *Nature* **420**, 414–418 (2002).
4. E. Slomowitz *et al.*, Interplay between population firing stability and single neuron dynamics in hippocampal networks. *eLife* **4**, e04378 (2015).
5. I. Vertkin *et al.*, GABAB receptor deficiency causes failure of neuronal homeostasis in hippocampal networks. *Proc. Natl. Acad. Sci. U.S.A.* **112**, E3291–E3299 (2015).
6. B. Styr *et al.*, Mitochondrial regulation of the hippocampal firing rate set point and seizure susceptibility. *Neuron* **102**, 1009–1024.e8 (2019).
7. K. B. Hengen, A. Torrado Pacheco, J. N. McGregor, S. D. Van Hooser, G. G. Turrigiano, Neuronal firing rate homeostasis is inhibited by sleep and promoted by wake. *Cell* **165**, 180–191 (2016).
8. K. B. Hengen, M. E. Lambo, S. D. Van Hooser, D. B. Katz, G. G. Turrigiano, Firing rate homeostasis in visual cortex of freely behaving rodents. *Neuron* **80**, 335–342 (2013).
9. T. Keck *et al.*, Synaptic scaling and homeostatic plasticity in the mouse visual cortex in vivo. *Neuron* **80**, 327–334 (2013).
10. A. Torrado Pacheco, J. Bottorff, Y. Gao, G. G. Turrigiano, Sleep promotes downward firing rate homeostasis. *Neuron* **109**, 530–544.e6 (2020).
11. G. W. Davis, M. Müller, Homeostatic control of presynaptic neurotransmitter release. *Annu. Rev. Physiol.* **77**, 251–270 (2015).
12. G. Turrigiano, Too many cooks? Intrinsic and synaptic homeostatic mechanisms in cortical circuit refinement. *Annu. Rev. Neurosci.* **34**, 89–103 (2011).
13. K. Pozo, Y. Goda, Unraveling mechanisms of homeostatic synaptic plasticity. *Neuron* **66**, 337–351 (2010).
14. M. B. Ramocki, H. Y. Zoghbi, Failure of neuronal homeostasis results in common neuropsychiatric phenotypes. *Nature* **455**, 912–918 (2008).
15. E. T. Kavalali, L. M. Monteggia, Targeting homeostatic synaptic plasticity for treatment of mood disorders. *Neuron* **106**, 715–726 (2020).
16. S. Frere, I. Slutsky, Alzheimer's disease: From firing instability to homeostasis network collapse. *Neuron* **97**, 32–58 (2018).
17. A. Ruggiero, M. Katsenelson, I. Slutsky, Mitochondria: New players in homeostatic regulation of firing rate set points. *Trends Neurosci.* **44**, 605–618 (2021).
18. G. LeMasson, E. Marder, L. F. Abbott, Activity-dependent regulation of conductances in model neurons. *Science* **259**, 1915–1917 (1993).
19. T. O'Leary, A. H. Williams, A. Franci, E. Marder, Cell types, network homeostasis, and pathological compensation from a biologically plausible ion channel expression model. *Neuron* **82**, 809–821 (2014).
20. S. J. Barnes *et al.*, Subnetwork-specific homeostatic plasticity in mouse visual cortex in vivo. *Neuron* **86**, 1290–1303 (2015).
21. A. J. D'Ercole, P. Ye, A. S. Calikoglu, G. Gutierrez-Ospina, The role of the insulin-like growth factors in the central nervous system. *Mol. Neurobiol.* **13**, 227–255 (1996).
22. A. M. Fernandez, I. Torres-Alemán, The many faces of insulin-like peptide signalling in the brain. *Nat. Rev. Neurosci.* **13**, 225–239 (2012).
23. C. Kenyon, J. Chang, E. Gensch, A. Rudner, R. Tabtiang, A *C. elegans* mutant that lives twice as long as wild type. *Nature* **366**, 461–464 (1993).
24. M. Holzenberger *et al.*, IGF-1 receptor regulates lifespan and resistance to oxidative stress in mice. *Nature* **421**, 182–187 (2003).
25. C. J. Kenyon, The genetics of ageing. *Nature* **464**, 504–512 (2010).
26. Y. Suh *et al.*, Functionally significant insulin-like growth factor I receptor mutations in centenarians. *Proc. Natl. Acad. Sci. U.S.A.* **105**, 3438–3442 (2008).
27. A. R. Mardinly *et al.*, Sensory experience regulates cortical inhibition by inducing IGF1 in VIP neurons. *Nature* **531**, 371–375 (2016).
28. D. Tropea *et al.*, Gene expression changes and molecular pathways mediating activity-dependent plasticity in visual cortex. *Nat. Neurosci.* **9**, 660–668 (2006).
29. J. F. Maya-Vetencourt *et al.*, IGF-1 restores visual cortex plasticity in adult life by reducing local GABA levels. *Neural Plast.* **2012**, 250421 (2012).
30. J. L. Trejo, E. Carro, I. Torres-Alemán, Circulating insulin-like growth factor I mediates exercise-induced increases in the number of new neurons in the adult hippocampus. *J. Neurosci.* **21**, 1628–1634 (2001).
31. Z. Chaker, S. Aïd, H. Berry, M. Holzenberger, Suppression of IGF-I signals in neural stem cells enhances neurogenesis and olfactory function during aging. *Aging Cell* **14**, 847–856 (2015).
32. Z. Chaker *et al.*, Hypothalamic neurogenesis persists in the aging brain and is controlled by energy-sensing IGF-I pathway. *Neurobiol. Aging* **41**, 64–72 (2016).
33. P. Cao, A. Maximov, T. C. Südhof, Activity-dependent IGF-1 exocytosis is controlled by the Ca(2+)-sensor synaptotagmin-10. *Cell* **145**, 300–311 (2011).
34. N. Gazit *et al.*, IGF-1 receptor differentially regulates spontaneous and evoked transmission via mitochondria at hippocampal synapses. *Neuron* **89**, 583–597 (2016).
35. A. Pristerà *et al.*, Dopamine neuron-derived IGF-1 controls dopamine neuron firing, skill learning, and exploration. *Proc. Natl. Acad. Sci. U.S.A.* **116**, 3817–3826 (2019).
36. L. E. Maglio *et al.*, IGF-1 facilitates extinction of conditioned fear. *eLife* **10**, e67267 (2021).
37. D. De Stefani, R. Rizzuto, T. Pozzan, Enjoy the trip: Calcium in mitochondria back and forth. *Annu. Rev. Biochem.* **85**, 161–192 (2016).
38. M. Holzenberger *et al.*, Experimental IGF-I receptor deficiency generates a sexually dimorphic pattern of organ-specific growth deficits in mice, affecting fat tissue in particular. *Endocrinology* **142**, 4469–4478 (2001).
39. F. Hakuno, S.-I. Takahashi, IGF1 receptor signaling pathways. *J. Mol. Endocrinol.* **61**, T69–T86 (2018).
40. F. Asztely, G. Erdemli, D. M. Kullmann, Extrasynaptic glutamate spillover in the hippocampus: Dependence on temperature and the role of active glutamate uptake. *Neuron* **18**, 281–293 (1997).
41. J. M. Christie, C. E. Jahr, Multivesicular release at Schaffer collateral–CA1 hippocampal synapses. *J. Neurosci.* **26**, 210–216 (2006).
42. I. Slutsky, S. Sadeghpour, B. Li, G. Liu, Enhancement of synaptic plasticity through chronically reduced Ca^{2+} flux during uncorrelated activity. *Neuron* **44**, 835–849 (2004).
43. O. Kann, R. Kovács, Mitochondria and neuronal activity. *Am. J. Physiol. Cell. Physiol.* **292**, C641–C657 (2007).
44. H. Imamura *et al.*, Visualization of ATP levels inside single living cells with fluorescence resonance energy transfer-based genetically encoded indicators. *Proc. Natl. Acad. Sci. U. S. A.* **106**, 15651–15656 (2009).
45. M. Patron, V. Granatiero, J. Espino, R. Rizzuto, D. De Stefani, MICU3 is a tissue-specific enhancer of mitochondrial calcium uptake. *Cell Death Differ.* **26**, 179–195 (2019).
46. L. F. Abbott, S. B. Nelson, Synaptic plasticity: Taming the beast. *Nat. Neurosci.* **3** (suppl.), 1178–1183 (2000).
47. G. G. Turrigiano, S. B. Nelson, Homeostatic plasticity in the developing nervous system. *Nat. Rev. Neurosci.* **5**, 97–107 (2004).
48. G. W. Davis, Homeostatic control of neural activity: From phenomenology to molecular design. *Annu. Rev. Neurosci.* **29**, 307–323 (2006).
49. T. O'Leary, Homeostasis, failure of homeostasis and degenerate ion channel regulation. *Curr. Opin. Physiol.* **2**, 129–138 (2018).
50. E. Marder, Variability, compensation, and modulation in neurons and circuits. *Proc. Natl. Acad. Sci. U.S.A.* **108** (Suppl. 3), 15542–15548 (2011).
51. A. A. Prinz, D. Bucher, E. Marder, Similar network activity from disparate circuit parameters. *Nat. Neurosci.* **7**, 1345–1352 (2004).
52. E. Marder, J. M. Goaillard, Variability, compensation and homeostasis in neuron and network function. *Nat. Rev. Neurosci.* **7**, 563–574 (2006).
53. E. Cohen *et al.*, Reduced IGF-1 signaling delays age-associated proteotoxicity in mice. *Cell* **139**, 1157–1169 (2009).
54. E. Cohen, J. Bieschke, R. M. Perciavalle, J. W. Kelly, A. Dillin, Opposing activities protect against age-onset proteotoxicity. *Science* **313**, 1604–1610 (2006).
55. J. E. Lisman, Bursts as a unit of neural information: Making unreliable synapses reliable. *Trends Neurosci.* **20**, 38–43 (1997).
56. M. L. Demory *et al.*, Epidermal growth factor receptor translocation to the mitochondria: Regulation and effect. *J. Biol. Chem.* **284**, 36592–36604 (2009).
57. T.-F. Che *et al.*, Mitochondrial translocation of EGFR regulates mitochondria dynamics and promotes metastasis in NSCLC. *Oncotarget* **6**, 37349–37366 (2015).

58. Y. Ding *et al.*, Receptor tyrosine kinase ErbB2 translocates into mitochondria and regulates cellular metabolism. *Nat. Commun.* **3**, 1271 (2012).
59. Y. Lin *et al.*, Brain activity regulates loose coupling between mitochondrial and cytosolic Ca^{2+} transients. *Nat. Commun.* **10**, 5277 (2019).
60. G. Csordás *et al.*, MICU1 controls both the threshold and cooperative activation of the mitochondrial Ca^{2+} uniporter. *Cell Metab.* **17**, 976–987 (2013).
61. S. Marchi, P. Pinton, The mitochondrial calcium uniporter complex: Molecular components, structure and physiopathological implications. *J. Physiol.* **592**, 829–839 (2014).
62. K. J. Kamer, V. K. Mootha, The molecular era of the mitochondrial calcium uniporter. *Nat. Rev. Mol. Cell Biol.* **16**, 545–553 (2015).
63. Ö. Genç *et al.*, MCTP is an ER-resident calcium sensor that stabilizes synaptic transmission and homeostatic plasticity. *eLife* **6**, e22904 (2017).
64. G. W. Davis, Homeostatic signaling and the stabilization of neural function. *Neuron* **80**, 718–728 (2013).
65. C. P. Goold, G. W. Davis, The BMP ligand Gbb gates the expression of synaptic homeostasis independent of synaptic growth control. *Neuron* **56**, 109–123 (2007).
66. C. C. Steinmetz, G. G. Turrigiano, Tumor necrosis factor-α signaling maintains the ability of cortical synapses to express synaptic scaling. *J. Neurosci.* **30**, 14685–14690 (2010).
67. O. Paulsen, T. J. Sejnowski, Natural patterns of activity and long-term synaptic plasticity. *Curr. Opin. Neurobiol.* **10**, 172–179 (2000).
68. O. Stoler *et al.*, Frequency- and spike-timing-dependent mitochondrial Ca^{2+} signaling regulates the metabolic rate and synaptic efficacy in cortical neurons. *eLife* **11**, e74606 (2022).
69. S. S. Divakaruni *et al.*, Long-term potentiation requires a rapid burst of dendritic mitochondrial fission during induction. *Neuron* **100**, 860–875.e7 (2018).
70. R. C. Malenka, M. F. Bear, LTP and LTD: An embarrassment of riches. *Neuron* **44**, 5–21 (2004).
71. T. O'Leary, M. C. W. van Rossum, D. J. A. Wyllie, Homeostasis of intrinsic excitability in hippocampal neurones: Dynamics and mechanism of the response to chronic depolarization. *J. Physiol.* **588**, 157–170 (2010).
72. B. Li *et al.*, Neuronal inactivity co-opts LTP machinery to drive potassium channel splicing and homeostatic spike widening. *Cell* **181**, 1547–1565.e1515 (2020).
73. K. Schaukowitch *et al.*, An intrinsic transcriptional program underlying synaptic scaling during activity suppression. *Cell Rep.* **18**, 1512–1526 (2017).
74. D. G. Wheeler *et al.*, Ca(V)1 and Ca(V)2 channels engage distinct modes of Ca(2+) signaling to control CREB-dependent gene expression. *Cell* **149**, 1112–1124 (2012).
75. G. M. Edelman, J. A. Gally, Degeneracy and complexity in biological systems. *Proc. Natl. Acad. Sci. U.S.A.* **98**, 13763–13768 (2001).
76. V. Tatavarty *et al.*, Autism-associated Shank3 is essential for homeostatic compensation in rodent V1. *Neuron* **106**, 769–777.e4 (2020).
77. A. Shcheglovitov *et al.*, SHANK3 and IGF1 restore synaptic deficits in neurons from 22q13 deletion syndrome patients. *Nature* **503**, 267–271 (2013).
78. J. Castro *et al.*, Functional recovery with recombinant human IGF1 treatment in a mouse model of Rett Syndrome. *Proc. Natl. Acad. Sci. U.S.A.* **111**, 9941–9946 (2014).
79. D. Tropea *et al.*, Partial reversal of Rett Syndrome-like symptoms in MeCP2 mutant mice. *Proc. Natl. Acad. Sci. U.S.A.* **106**, 2029–2034 (2009).
80. M. P. Blackman, B. Djukic, S. B. Nelson, G. G. Turrigiano, A critical and cell-autonomous role for MeCP2 in synaptic scaling up. *J. Neurosci.* **32**, 13529–13536 (2012).
81. Z. Qiu *et al.*, The Rett syndrome protein MeCP2 regulates synaptic scaling. *J. Neurosci.* **32**, 989–994 (2012).
82. V. S. Dani *et al.*, Reduced cortical activity due to a shift in the balance between excitation and inhibition in a mouse model of Rett syndrome. *Proc. Natl. Acad. Sci. U.S.A.* **102**, 12560–12565 (2005).
83. G. Gontier, C. George, Z. Chaker, M. Holzenberger, S. Aïd, Blocking IGF signaling in adult neurons alleviates Alzheimer's disease pathology through amyloid-β clearance. *J. Neurosci.* **35**, 11500–11513 (2015).
84. S. Freude *et al.*, Neuronal IGF-1 resistance reduces Abeta accumulation and protects against premature death in a model of Alzheimer's disease. *FASEB J.* **23**, 3315–3324 (2009).
85. M. Calvo-Rodriguez, B. J. Bacskai, Mitochondria and calcium in Alzheimer's disease: From cell signaling to neuronal cell death. *Trends Neurosci.* **44**, 136–151 (2020)
86. D. Pozzi *et al.*, REST/NRSF-mediated intrinsic homeostasis protects neuronal networks from hyperexcitability. *EMBO J.* **32**, 2994–3007 (2013).
87. J. M. Zullo *et al.*, Regulation of lifespan by neural excitation and REST. *Nature* **574**, 359–364 (2019).
88. M. Holzenberger *et al.*, A targeted partial invalidation of the insulin-like growth factor I receptor gene in mice causes a postnatal growth deficit. *Endocrinology* **141**, 2557–2566 (2000).
89. E. Abramov *et al.*, Amyloid-beta as a positive endogenous regulator of release probability at hippocampal synapses. *Nat. Neurosci.* **12**, 1567–1576 (2009).
90. N. R. Sims, M. F. Anderson, Isolation of mitochondria from rat brain using Percoll density gradient centrifugation. *Nat. Protoc.* **3**, 1228–1239 (2008).